Role of Asp[1393] in Catalysis, Flavin Reduction, NADP(H) Binding, FAD Thermodynamics, and Regulation of the nNOS Flavoprotein†

David W. Konas,‡,§ Naoki Takaya,‡,|| Manisha Sharma, and Dennis J. Stuehr*

Department of Pathobiology, The Lerner Research Institute, The Cleveland Clinic Foundation, Cleveland, Ohio 44195

Received May 21, 2006; Revised Manuscript Received July 14, 2006

ABSTRACT: Nitric oxide synthases (NOS) are flavoheme enzymes with important roles in biology. The reductase domain of neuronal NOS (nNOSr) contains a widely conserved acidic residue (Asp[1393]) that is thought to facilitate hydride transfer between NADPH and FAD. Previously we found that the D1393V and D1393N mutations lowered the NO synthesis activity and the rates of heme and flavin reduction in full-length nNOS. To examine the mechanisms for these results in greater detail, we incorporated D1393V and D1393N substitutions into nNOSr along with a truncated NADPH-FAD domain construct (FNR) and characterized the mutants. D1393V nNOSr had markedly lower ($\leq$1000×) cytochrome *c* reductase, ferricyanide reductase, and NADPH oxidase activities than the wild type. D1393N nNOSr also had lower reductase activities ($\leq$10×) but had greater NADPH oxidase activity than that of the wild type, as did its FNR fragment. Both mutants had an altered interaction between FAD and the nicotinamide ring of $NADP^+$, slower flavin reduction by NADPH, altered FAD midpoint potentials, a normal CaM response, and, in one case (D1393N), faster flavin oxidation by O_2 and a lack of FMN shielding in response to NADPH binding. The results suggest that the two mutants have compromised catalysis for two different reasons. In D1393V nNOSr, hydride transfer from NADPH to FAD is so slow that it compromises all downstream electron-transfer events. In D1393N nNOSr, the increased oxidation of reduced flavins by O_2 and thermodynamic destabilization of the FAD semiquinone uncouples or limits electron transfer to an extent that it inhibits downstream catalysis. These effects are due in part to the mutations eliminating (D1393V) or altering (D1393N) the native side-chain hydrogen-bonding properties of Asp[1393] as well as removing its negative charge.

The free radical nitric oxide (NO) is a physiologically important molecule because of its involvement in cardiovascular and neuronal function, inflammation, and immunity (*1*, *2*). NO is produced enzymatically in mammalian cells by three isoforms of nitric oxide synthase (NOS[1]) (*3*, *4*). NOS catalyzes the monooxygenation of L-arginine yielding N^{ω}-hydroxy-L-arginine, which is subsequently monooxygenated to form the final products: L-citrulline and NO. The site for arginine binding is located in a protein structural domain known as the *N*-terminal oxygenase domain. The oxygenase domain also contains protoporphyrin IX (heme) and a second cofactor, tetrahydrobiopterin (H_4B) (*5*). Electrons are provided to the heme in the *N*-terminal oxygenase domain by a *C*-terminal reductase domain (NOSr). The NOSr obtains electrons from NADPH and shuttles them between bound FAD and FMN cofactors in order to produce a 2-electron reduced FMN hydroquinone ($FMNH_2$), which is the species required for NOS heme reduction. NOSr's belong to a family of structurally related diflavin reductases, which also includes cytochrome P450 reductase (P450R) (*6*, *7*), methionine synthase reductase (*8*), and novel reductase-1 (*9*). These flavoproteins all contain two distinct subdomains. One subdomain contains the binding sites for NADPH and FAD and is structurally similar to ferredoxin-$NADP^+$ reductases (FNR) (*10*). The other subdomain contains the FMN cofactor and is structurally similar to flavodoxins (*11*). Despite their structural similarity, it is important to appreciate that NOSr possess the additional complexities of an internal regulatory system not found in proteins such as P450R. For example, rates of NOSr electron-transfer reactions are, with the exception of novel reductase-1 (*12*), repressed relative to those of other related flavoproteins, but CaM binding relieves this repression. The CaM-induced de-repression of electron transfer is associated with a de-shielding of the FMN cofactor within nNOSr (*13*, *14*). This forms the basis for the hypothesis that electron transfer from nNOSr is regulated in part by the position of a dynamic equilibrium that determines the relative amounts of shielded or de-shielded FMN cofactor (*14*). In addition to CaM binding, other components involved in regulating NOSr electron transfer include an autoinhibitory

† This work was supported by National Institute of Health Grants GM51491 and HL76491 (to D.J.S.).

* Author to whom correspondence should be addressed. Phone: (216)-445-6950. Fax: (216)-444-9329. E-mail: stuehrd@ccf.org.

‡ These authors contributed equally to this work.

§ Current address: Department of Chemistry and Biochemistry, Montclair State University, Montclair, NJ, 07043.

|| Current address: Graduate School of Life and Environmental Science, University of Tsukuba, Tsukuba, Ibaraki 305-8572, Japan.

[1] Abbreviations: CaM, calmodulin; EPPS, 4-(2-hydroxyethyl)-1-piperazinepropanesulfonic acid; FNR, ferredoxin $NADP^+$ reductase; NOS, nitric oxide synthase; nNOS, neuronal NOS; nNOSr, reductase (flavoprotein) domain of nNOS; nNOSfnr, FNR domain of nNOS; P450R, cytochrome P450 reductase.

10.1021/bi061011t CCC: $33.50
Published on Web 09/26/2006

sequence within the FMN domain (*15*−*18*), a *C*-terminal extension (*19*−*21*), multiple phosphorylation sites (*22*−*27*), a loop within the connecting domain (*28*), a conserved Phe residue, which stacks against the FAD isoalloxazine ring and governs the NADPH nicotinamide interaction (*14*, *29*), and NADP(H) binding (*13*, *30*). How these regulatory elements function or cooperate at the molecular level is a topic of current interest in NOS enzymology and general flavoprotein biochemistry.

NOSr's also contain structural elements in common with those of related flavoproteins that participate in fundamental aspects of their electron-transfer reactions. For example, sequence comparisons of FNR and FNR-like proteins reveal three conserved amino acids (Cys, Ser, and Asp/Glu) located near the FAD cofactor, sometimes referred to as a catalytic triad. The specific residues comprising the catalytic triad of nNOSr are Cys^{1349}, Ser^{1176}, and Asp^{1393} (*31*). Crystal structures of FNR (*32*), P450R (*6*), and neuronal NOSr (nNOSr) (*31*, *33*) reveal that these amino acids form a hydrogen bond network adjacent to the FAD cofactor and the NADPH binding site. These structural data suggest potential roles for the triad in facilitating proton transfers associated with FAD oxidation/reduction, the proper positioning of bound NADPH, and in determining FAD thermodynamic properties. However, the proximity of the catalytic triad to the Phe^{1395} and *C*-terminal tail regulatory elements in nNOSr raises the possibility of its involvement in the internal regulatory system. We recently reported the effects of point mutations of Asp^{1393} in full-length nNOS (*34*). Our results demonstrated that these nNOS mutants (D1393V, N, and E) had significantly decreased flavin reduction kinetics and steady-state catalytic activities (NO synthesis, cytochrome *c* reduction). These variations from typical wild-type nNOS kinetics are mainly attributed to changes or defects in NADPH-FAD hydride transfer and/or FAD−FMN interflavin electron transfer, depending on the particular mutation involved. The conclusions drawn from these studies were possible because of data obtained from experiments designed to take advantage of the attached oxygenase (heme) domain present in full-length nNOS. Because heme reduction in nNOS is carried out only by $FMNH_2$, the heme redox state provided a built-in reporter of FMN redox status in mutants where heme reduction is fast relative to flavin reduction kinetics. Unfortunately, the presence of a catalytically active oxygenase domain is problematic for other experiments designed to examine nNOSr properties and the internal regulatory system in detail. The relatively large heme absorbance spectrum has significant overlap with the less intense flavin absorbance region, and the heme also provides a sometimes unwanted pathway for electrons to leave the reductase domain in the CaM-bound protein. For this reason, studies of nNOSr and its regulatory elements frequently utilize constructs containing only the flavoprotein and its adjacent CaM-binding motif (*13*, *14*, *35*−*39*). Individual nNOSr subdomains, such as the FNR-like (nNOSfnr) subdomain, can also be obtained and studied in this way (*31*, *39*, *40*). The dramatic impact of Asp^{1393} mutations on the properties of nNOS (*34*) prompted us to study two mutations (D1393V, D1393N) in the context of isolated nNOSr and nNOSfnr subdomains. Our current results provide a greater understanding of Asp^{1393} regarding its functional roles in electron transfer, NADP(H) binding, FAD thermodynamics, and the nNOSr internal regulatory system.

EXPERIMENTAL PROCEDURES

General Materials and Methods. All reagents and materials were obtained from Sigma, Alexis Biochemicals, Amersham Biosciences, or other sources as previously reported (*14*). General experimental methods and equipment used were as previously reported (*14*), unless noted otherwise. The calculated best-fit lines of stopped-flow data were essentially indistinguishable from the actual data, unless noted or shown otherwise.

Generation and Purification of nNOSr Proteins. D1393V and D1393N mutations were prepared on the basis of our wild-type rat nNOSr construct within the pCWori vector as previously described (*14*) using the following PCR primers: D1393V forward primer, 5′-AACGGTACCACGAG**GT-C**ATCTTTGGAGTCACCCTCAGAACG-3′; D1393N forward primer, 5′-AACGGTACCACGAG**AAC**ATCTTTGGAGTCACCCTCAGAACG-3′; and reverse primer, 5′-AAATCTAGAAGGACCAGGACACAGCAACAGGACAAG-3′. The restriction sites are underlined and the mutation sites are indicated with bold underlining. The proteins were coexpressed with pACYC CaM in *Escherichia coli* BL21-(DE3) cells as previously described (*14*). Proteins were purified as previously described (*14*) by sequential affinity chromatography steps using 2′-,5′-ADP sepharose and CaM sepharose, with the exception that D1393N nNOSr samples used for biochemical studies were eluted from the 2′-,5′-ADP sepharose column using 10 mM 2′-AMP instead of NADPH (see Results). The isolated FAD−NADPH subdomains (nNOSfnr) of wild type and mutant nNOSr were prepared as follows. The purified nNOSr proteins (typically 50 to 200 nmol) were treated with trypsin (134 U/μL) at room temperature for 2 h. The reactions were stopped with 1 mM phenylmethylsulfonyl fluoride, and the proteolytically generated nNOSfnr proteins were purified by 2′-,5′-ADP sepharose column chromatography as described above for each nNOSr. The nNOSfnr proteins appeared as single bands upon analysis by SDS−PAGE. *N*-terminal sequencing revealed that nNOSfnr began at rat nNOS amino acid 987 with the sequence ANNSLI. The apparent molecular weight was approximately 52 kDa, corresponding very well to the expected value with the knowledge that the nNOSfnr proteins prepared in this manner are truncated by 22 amino acids at the *C*-terminal end (*31*, *40*). The purified nNOSr and nNOSfnr proteins were oxidized with potassium ferricyanide and either dialyzed extensively against Buffer A (40 mM EPPS, pH 7.6, 150 mM NaCl, 10% glycerol) or passed through a PD-10 rapid gel filtration column followed by flash freezing and storage at −80 °C. The concentrations of oxidized proteins were determined spectrophotometrically using the extinction coefficients (457 nm) of 22.9 mM^{-1} cm^{-1} for nNOSr and 10.2 mM^{-1} cm^{-1} (*39*) for nNOSfnr.

Steady-State Assays. Steady-state NADPH-ferricyanide reductase, NADPH-cytochrome *c* reductase, and NADPH oxidase activities were measured in the presence of superoxide dismutase and catalase at 25 °C as described previously (*41*). Apparent K_m values for NADPH were determined by fitting standard double reciprocal plots of NADPH-cytochrome *c* reductase activity versus NADPH concentration.

Determination of Bound Flavin Content. Protein samples were boiled for 5 min in the dark and the precipitated protein was collected by centrifugation. Total flavin concentration in the supernatant was determined using the extinction coefficient of 12.2 mM^{-1} cm^{-1} at 447 nm. The ratio of FAD and FMN was determined using an HPLC method as previously described (*41*).

Interaction between nNOSr Proteins and NADP$^+$. Visible spectral changes resulting from the association of $NADP^+$ with the nNOSr proteins were evaluated as previously reported (*14*).

Anaerobic Stopped-Flow Flavin Reduction Kinetics. Stopped-flow rapid scan analysis of flavin reduction by excess NADPH was performed under anaerobic conditions at 10 °C using a HiTech Ltd. SF-61 (Salisbury, U.K.) apparatus with diode-array detection. Single wavelength data was obtained using a HiTech Ltd. SF-51MX equipped with photomultiplier detection. The procedure used was similar to that described previously (*14*). Briefly, the fully oxidized wild-type and mutant proteins were diluted to 10 μM (for nNOSr) or 20 μM (for nNOSfnr) with Buffer A containing EDTA (1 mM), glucose oxidase (10 U/mL), catalase (134 U/mL), and glucose (2 mM) and then rapidly mixed with 100 μM (for nNOSr) or 200 μM (for nNOSfnr) NADPH in Buffer A. To analyze CaM-bound samples, EDTA was replaced with $CaCl_2$ (2 mM) and CaM (15 μM). Averaged absorbance changes at 458 and 600 nm were fit to single or multiple exponential functions using software provided by the instrument manufacturer as indicated in the text.

Anaerobic Presteady-State Cytochrome c Reduction. The rate of reduction of cytochrome *c* by an excess of prereduced nNOSr proteins under various conditions was measured in the stopped-flow apparatus (HiTech Ltd. SF-51MX) at 10 °C as previously described (*14*). Briefly, each nNOSr wild-type or mutant protein (16 μM) in Buffer A containing EDTA (1 mM), 5-deazariboflavin (catalytic), glucose oxidase (10 U/mL), catalase (134 U/mL), and glucose (2 mM) was completely photoreduced in a sealed cuvette. To analyze CaM-bound samples, EDTA was replaced with glycine, and $CaCl_2$ (2 mM) and CaM (25 μM) were included. In some cases, the photoreduced proteins were incubated with NADPH, and then rapidly mixed with cytochrome *c* (4 μM) while recording the absorbance changes at 550 nm. Multiple absorbance traces were averaged and fit to a single-exponential function.

Redox Potentiometry. Flavin equilibrium midpoint redox potentials of nNOSfnr were determined in an anaerobic glass cuvette essentially as previously described (*42*). The protein solution (40−60 μM in potassium phosphate (100 mM, pH 7.0), 10% glycerol, 0.5% Tween 20, EDTA (1 mM), 2-hydroxy-1,4-napthoquinone (0.5 μM), and methyl viologen (0.5 μM)) was made anaerobic with repeated vacuum/N_2 flush cycles and titrated with sodium dithionite as a reductant and potassium ferricyanide as an oxidant. The electrochemical potential was measured at 25 °C using a silver/silver chloride electrode calibrated using the Fe^{2+}/Fe^{3+} couple as a standard ($E_m = +425$ mV). Absorption spectra measuring the titration progress were recorded after the system potential became stable (more than 15 min). The midpoint potentials were calculated using the absorbance change at 458 (for mutants and wild type) and 600 nm (for wild type) by fitting to the following two-electron Nernst equation (*12*):

$$A = [a10^{(E-E1')/59} + b + c10^{(E2'-E)/59}]/[1 + 10^{(E-E1')/59} + 10^{(E2'-E)/59}]$$

where A is absorption, $a-c$ are the relative absorbance values of FAD in each redox state (oxidized, semiquinone, and hydroquinone), E is the observed system potential, and $E1$ and $E2$ are the two equilibrium midpoint potentials (oxidized/semiquinone and semiquinone/hydroquinone).

Oxidation of Prereduced nNOSr Proteins by Excess Cytochrome c. The rate of reduction of excess cytochrome *c* by prereduced nNOSr proteins was measured in the stopped-flow apparatus (HiTech Ltd. SF-51MX) at 10 °C. Each nNOSr wild-type or mutant protein (10 μM) in Buffer A containing EDTA (3 mM) and 5-deazariboflavin (catalytic) was photoreduced in a sealed cuvette and mixed with a solution of cytochrome *c* (100 μM) while monitoring the absorbance changes at 550 nm. Multiple absorbance traces were averaged and fit to a multiple exponential function as appropriate.

Autooxidation of Reduced Flavins. Solutions of WT and D1393N nNOSr (8 μM) in air-saturated Buffer A were reduced by adding NADPH (160 μM), and then they were allowed to autooxidize at room temperature in an open cuvette. The process was monitored by recording the absorbance changes at 457 nm versus time during the experiment.

RESULTS

Purification and Catalytic Properties of Asp^{1393} Mutants. To examine the specific roles of Asp^{1393} within the reductase domain, we expressed and purified nNOSr proteins in which Asp^{1393} was replaced with either Val or Asn (nNOSr D1393V and nNOSr D1393N, respectively). FMN and FAD were incorporated into each of the proteins in approximately the expected 1:1 ratio, indicating that the mutations did not grossly alter the structure and flavin-binding properties of nNOSr. Absorption spectra of the oxidized mutant proteins contained maxima at 387, 457, and 480 nm and were not distinguishable from the spectrum of wild-type (WT) nNOSr (data not shown). Upon addition of a substoichiometric amount of either NADPH or sodium dithionite under aerobic conditions, the mutants exhibited a loss of absorbance at 457 nm and gained a broad absorption peak centered near 600 nm. These spectral properties are characteristic of the air-stable FMN semiquinone form of WT nNOSr and other related flavoproteins. In the case of the D1393N mutant, however, this semiquinone was not air-stable, and it slowly reoxidized. Accordingly, D1393N nNOSr was obtained in its fully oxidized form following the purification procedure. In addition, when nNOSr D1393N was purified by 2′,5′-ADP sepharose affinity chromatography and eluted with 10 mM NADPH, the resulting protein contained no FAD. In its place was another yellow compound with an absorption spectrum similar to that observed for 6-hydroxy FAD (Takaya, N. and Stuehr, D., unpublished results) (*43*). This phenomenon was not observed in D1393V nNOSr or WT nNOSr, indicating that subtle changes in the Asp^{1393} residue may affect its flavin-binding characteristics or perhaps create the ability of the mutant to modify its own cofactors, as occurs in the human apoptosis-inducing flavoprotein AMID (*44*). To verify that the formation of 6-hydroxy FAD in

Table 1: Steady-State Activities of WT and Mutant nNOSr and nNOSfnr Proteins[a]

protein	conditions	cytochrome *c* reductase	ferricyanide reductase	NADPH oxidase
WT nNOSr	−CaM	455 ± 9	1505 ± 29	14 ± 2
WT nNOSr	+CaM	3930 ± 202 (8.6)	2900 ± 201 (1.9)	80 ± 5 (5.7)
D1393V nNOSr	−CaM	0.8 ± 0.02	7.5 ± 0.2	0.9 ± 0.4
D1393V nNOSr	+CaM	2.2 ± 0.1 (2.7)	8.1 ± 0.4 (1.1)	1.0 ± 0.5 (1.1)
D1393N nNOSr	−CaM	216 ± 8.5	288 ± 11	75 ± 3
D1393N nNOSr	+CaM	679 ± 10.5 (3.1)	619 ± 46 (2.1)	288 ± 23 (3.8)
WT nNOSfnr	−CaM	3.0 ± 0.1	1570 ± 40	5.1 ± 0.5
D1393V nNOSfnr	−CaM	1.1 ± 0.1	3.5 ± 0.5	4.2 ± 0.2
D1393N nNOSfnr	−CaM	9.3 ± 0.6	720 ± 40	34 ± 1

[a] Activities were determined at 25 °C as described under Experimental Procedures, and the average values of at least four trials are reported as turnover number (min^{-1}) ± S.D. in each case. The value given after each +CaM turnover number is the ratio of +CaM activity to −CaM activity for that protein and assay combination

D1393N nNOSr did not take place under our typical experimental conditions utilizing NADPH, a sample of the enzyme was treated with 20 equiv of NADPH in air-saturated buffer until all the NADPH was consumed. The protein sample was denatured by boiling in the dark for 2 min, and the free flavins obtained were analyzed by reversed-phase HPLC. The results were essentially identical to those obtained when the same HPLC flavin analysis was carried out on both WT nNOSr and freshly purified D1393N nNOSr, indicating that the FAD cofactor had not been modified during catalysis.

Steady-state ferricyanide reductase, cytochrome *c* reductase, and NADPH oxidase activities of our mutant and WT nNOSr proteins are given in Table 1. In most cases, the activities of the mutants were lower than those observed for WT nNOSr, with the D1393V mutation having the greatest impact. This is consistent with our previous results obtained using full-length nNOS mutants (*34*). The major exception to this trend was the NADPH oxidase activities of D1393N nNOSr, which were over 5-fold (−CaM) and nearly 4-fold (+CaM) greater than the corresponding values obtained with WT nNOSr. The cytochrome *c* reductase activities of D1393N and D1393V nNOSr were stimulated 3.1- and 2.7-fold, respectively, by CaM binding. These effects of CaM on the mutants were less than that observed in WT nNOSr (8.6-fold). Apparent K_m values for NADPH in D1393N and D1393V nNOSr were measured using the cytochrome *c* reductase assay and found to be 0.50 ± 0.1 and 1.6 ± 0.2 μM in the absence of CaM and 0.83 ± 0.2 and 2.2 ± 0.2 μM in the presence of CaM, respectively. These values are comparable to those determined for WT nNOSr: 2.5 ± 0.5 μM (CaM-free) and 4.8 ± 0.2 μM (CaM-bound).

Kinetics and Characteristics of nNOSr Flavin Reductions by NADPH. We studied the reduction of our oxidized nNOSr proteins by excess NADPH under anaerobic conditions using stopped-flow spectroscopy. Absorbance changes at 458 nm for the reduction of WT nNOSr (data not shown), D1393V nNOSr (Figures 1, 2), and D1393N nNOSr (Figure 3) were fit with two or three rate constants as appropriate to give the values reported in Table 2. For the WT nNOSr and other flavin reduction experiments carried out in this study, the values of k_1-k_3 (Table 2) correspond to the first three (k_1-k_3) rate constants for WT nNOSr reported previously (*14*, *37*). A fourth rate constant can often be determined by analysis of the end of a complete flavin reduction experiment (*14*, *37*), but this value is not catalytically relevant. When compared to WT nNOSr, the flavin reduction rates obtained

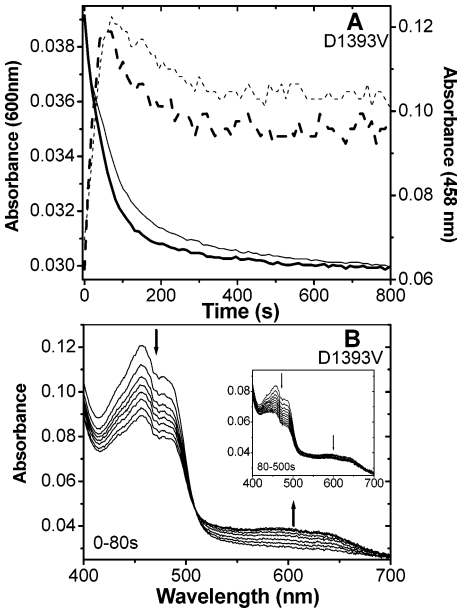

FIGURE 1: Stopped-flow data collected during anaerobic flavin reduction of fully oxidized D1393V nNOSr by a 10-fold excess of NADPH at 10 °C. Single wavelength data collected at 458 nm (solid lines) and 600 nm (dash lines) in the presence (thick lines) and absence (thin lines) of Ca^{+2}/CaM during a complete reduction experiment (800 s) are given in panel A. Rapid-scan diode array spectra corresponding to the reduction of CaM-free D1393V nNOSr collected during the 0−80 s time period are given in panel B. Rapid-scan diode array spectra corresponding to the same sample on an 80−500 s time scale are given in panel B, inset.

for the D1393V and D1393N nNOSr mutants were generally 1000- and 10-fold lower, respectively. This result is again consistent with our data collected using full-length nNOS proteins (*34*), and it implies that mutations of Asp^{1393} can affect both hydride transfer and interflavin electron transfer in nNOSr.

The slow reduction rates of the mutants enabled us to observe spectral intermediates appearing during the reaction and evaluate the flavin reduction process in each mutant with a level of detail impossible to achieve using full-length proteins. Absorbance changes occurring on an extended time scale corresponding to the reduction of the D1393V mutant by NADPH at 458 and 600 nm are given in Figure 1, panel A. An inspection of this data indicates that for approximately 80 s after initiating the reduction of D1393V nNOSr, we observed a decrease in absorbance at 458 nm accompanied by an increase of absorbance at 600 nm. A set of complete spectra corresponding to this phase of the reduction process

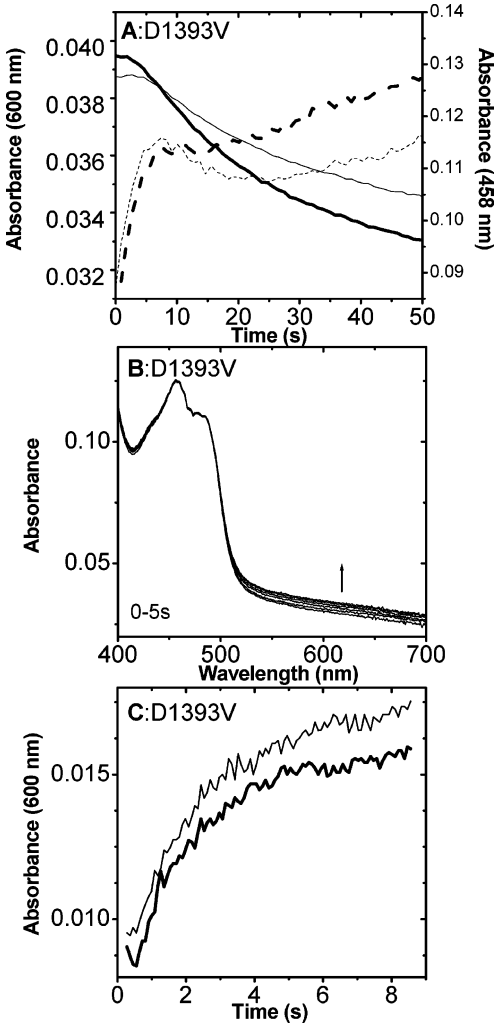

FIGURE 2: Stopped-flow data collected during the anaerobic flavin reduction of fully oxidized D1393V nNOSr by a 10-fold excess of NADPH at 10 °C. Single wavelength data collected at 458 nm (solid lines) and 600 nm (dash lines) in the presence (thick lines) and absence (thin lines) of Ca^{+2}/CaM during the 0−50 s phase of the reduction are given in panel A. Rapid-scan diode array spectra collected during the 0−5 s time period illustrating NADPH−FAD charge-transfer complex formation in CaM-free D1393V nNOSr are given in panel B. Single wavelength data at 600 nm obtained during NADPH−FAD charge-transfer complex formation (0−5 s) in the presence (thick lines) and absence (thin lines) of Ca^{+2}/CaM are given in panel C.

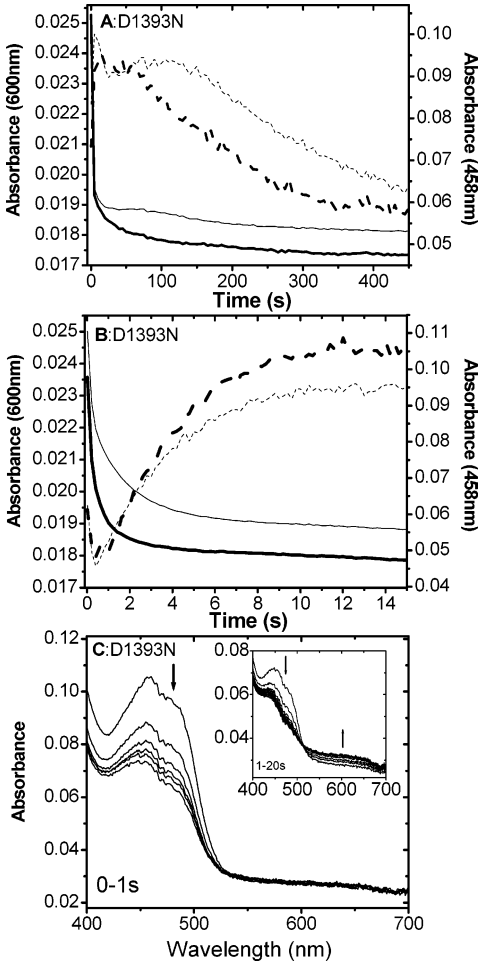

FIGURE 3: Stopped-flow data collected during the anaerobic flavin reduction of fully oxidized D1393N nNOSr by a 10-fold excess of NADPH at 10 °C. Single wavelength data collected at 458 nm (solid lines) and 600 nm (dash lines) in the presence (thick lines) and absence (thin lines) of Ca^{+2}/CaM during a complete reduction experiment (450 s) are given in panel A. Data collected during the first 15 s of this process are given in panel B with the same legend as that in panel A. Rapid-scan diode array spectra associated with reduction of CaM-free D1393N nNOSr during the 0−1 s time period are given in panel C, followed by complete spectra of the subsequent phase (1−20 s) given in panel C, inset.

is given in Figure 1, panel B for the CaM-free protein. These sequential spectra are characterized by a loss of absorbance at 458 nm (flavin reduction), the buildup of a broad absorbance band centered near 600 nm (semiquinone formation), an isosbestic point at 508 nm, and no significant absorbance changes at 700 nm. This stage of the reduction of D1393V nNOSr (Figure 1, panel B) can be correlated with the initial kinetic phase (k_1) calculated for the absorbance changes at 458 nm (0.014 s^{-1}, −CaM; 0.049 s^{-1}, +CaM; Table 2) and 600 nm (0.021 s^{-1}, −CaM; 0.034 s^{-1}, +CaM; Table 3). The corresponding rates at each wavelength have reasonably comparable values, consistent with the isosbestic point appearing between the two wavelengths. After completion of the first phase, the remainder of the reduction process was characterized by a decrease in absorbance at 600 nm (semiquinone reduction) and a continued decrease in absorbance at 458 nm. The calculated rates of these changes (k_2) are given in Tables 2 and 3, and full spectra corresponding to this second phase are shown in Figure 1, panel B (inset).

The initial phase of NADPH reaction with D1393V nNOSr, shown in Figure 2, reveals an additional aspect of this process. After mixing the enzyme and NADPH, a lag period (∼ 5−10 s) was observed before the decrease in absorbance at 458 nm was initiated (Figure 2, panel A). However, an increase in absorbance at 600 nm was observed without any lag. This initial increase at 600 nm reached a brief plateau until continuing with a larger increase corresponding to the semiquinone formation already described above in reference to Figure 1. An analysis of complete spectra collected during the lag period (Figure 2, panel B) showed that the increase at 600 nm is part of a broad, general absorbance increase extending past 700 nm into higher wavelength regions. This type of spectrum is characteristic of flavoprotein charge-transfer complexes (*45*). Because the formation of the charge-transfer complex is not accompanied by any absorbance decrease at 458 nm, this spectral intermediate must be an oxidized FAD−NADPH charge-

Table 2: Rates of Anaerobic Flavin Reduction of nNOSr and nNOSfnr Proteins by Excess NADPH at 458 nm[a]

protein	conditions	dead time[b] (%)	k_1[c] (%) (s^{-1})	k_2[c] (%) (s^{-1})	k_3[c] (%) (s^{-1})
WT nNOSr	−CaM	24	42 ± 6.0 (23)	7.2 ± 4.5 (23)	2.5 ± 0.7 (30)
WT nNOSr	+CaM	37	121 ± 10 (17)	16 ± 0.7 (26)	3.1 ± 0.1 (20)
D1393V nNOSr	−CaM	0	0.014 ± 0.0004 (76)	0.0025 ± 0.0003 (24)	
D1393V nNOSr	+CaM	0	0.049 ± 0.0003 (57)	0.018 ± 0.0002 (43)	
D1393N nNOSr	−CaM	0	4.3 ± 0.3 (44)	0.4 ± 0.01 (39)	0.008 ± 0.0002 (17)
D1393N nNOSr	+CaM	0	6.9 ± 0.3 (44)	1.2 ± 0.04 (39)	0.009 ± 0.0004 (17)
WT nNOSfnr	−CaM	9	68 ± 2.0 (59)	11 ± 0.3 (32)	
D1393Vfnr	−CaM	11	0.04 ± 0.002 (89)		
D1393Nfnr	−CaM	10	36 ± 6.0 (62)	12 ± 0.1 (13)	0.17 ± 0.01 (15)

[a] Reductions were carried out in the stopped-flow instrument at 10 °C using an excess of NADPH while monitoring the absorbance changes at 458 nm. Data were fit to multiple exponential functions as described under Experimental Procedures. [b] Percentage of the total absorbance change occurring in the instrument dead time. [c] Individual rate constants are reported as follows: calculated rate (s^{-1}) (% of the total absorbance change for this process).

Table 3: Rates of Anaerobic Flavin Reduction of nNOSr Proteins by Excess NADPH at 600 nm[a]

protein	conditions	k_1 (s^{-1})	k_2 (s^{-1})
WT nNOSr	−CaM	36 ± 4	3.7 ± 0.3
WT nNOSr	+CaM	98 ± 13	7.1 ± 0.5
D1393V nNOSr	−CaM	0.021 ± 0.006	0.014 ± 0.005
D1393V nNOSr	+CaM	0.034 ± 0.5	0.014 ± 0.2
D1393N nNOSr	−CaM	0.30 ± 0.01	0.0044 ± 0.0003
D1393N nNOSr	+CaM	0.32 ± 0.01	0.0043 ± 0.0003

[a] Reductions were carried out in the stopped-flow instrument at 10 °C using an excess of NADPH while monitoring the absorbance changes at 600 nm. Data were fit to multiple exponential functions as described under Experimental Procedures to give rates of semiquinone formation (k_1) and reduction (k_2).

transfer complex formed prior to hydride transfer. Absorbance changes at 600 nm corresponding to formation of the FAD−NADPH charge-transfer complex are given in Figure 2, panel C. These data were fit to a single-exponential function, yielding rates of charge-transfer complex formation of 0.55 ± 0.05 s^{-1} (−CaM) and 0.46 ± 0.04 s^{-1} (+CaM) and demonstrating that there was no significant effect of CaM binding on FAD−NADPH charge-transfer complex formation in D1393V nNOSr.

Stopped-flow data obtained at 458 and 600 nm during the reduction of D1393N nNOSr by NADPH are given in Figure 3, panel A. Most (~83%) of the absorbance decrease at 458 nm occurred within 20 s in a biphasic process (k_1 and k_2, Table 2; Figure 3, panel B) followed by a much slower third reaction phase (k_3, Table 2), which was completed after nearly 500 s. CaM binding increased the calculated rates of k_1 and k_2 in D1393N nNOSr (Table 2) but had no effect on k_3. The first phase occurred within 1 s after mixing, and it involved 44% of the total absorbance change at 458 nm. Rapid-scan stopped-flow data collected for the CaM-free protein (Figure 3, panel C) demonstrate that the first phase of reduction of D1393N nNOSr was not accompanied by any significant absorbance changes in the 550−700 nm region. Therefore, this phase of the reaction involved hydride transfer from NADPH to form $FADH_2$, but no simultaneous interflavin electron transfer or charge-transfer complex formation took place. In the second phase of the reaction (~1−20 s), absorbance increases in the 550−700 nm range did occur (Figure 3, panel C, inset). On the basis of the characteristics of these spectra, the second phase involved the formation of flavin semiquinone species (possibly via intra and/or intermolecular electron transfer) and a charge transfer complex, most likely $FADH_2$−$NADP^+$. The continued loss of absorbance at 458 nm observed during the second phase indicates that further reduction of the flavins occurs during this phase. Last, the third phase involved a small amount of additional flavin reduction and thermodynamic equilibration of the system. During this final phase, an absorbance decrease at 600 nm corresponding to the reduction of the flavin semiquinone species took place (Figure 3, panel A). The time elapsed prior to semiquinone reduction was approximately doubled in the CaM-free protein compared to that in CaM-bound D1393N nNOSr.

Properties of WT and Mutant nNOSfnr. We prepared the FAD/NADPH binding subdomains of the nNOSr proteins (nNOSfnr) by limited proteolysis with trypsin (*31*). The steady-state electron transfer activities measured for these proteins are given in Table 1. The ferricyanide reductase activity of each nNOSfnr protein was either comparable to or larger than that measured for each of the corresponding CaM-free nNOSr proteins, reinforcing the concepts that catalytic reduction of ferricyanide takes place via the FAD cofactor, and the absence of the FMN subdomain may result in more facile interaction between ferricyanide in solution and enzyme-bound FAD. The turnover numbers for cytochrome *c* reduction by WT and D1393N nNOSfnr proteins were significantly less than the values for the corresponding nNOSr proteins, affirming the involvement of FMN in the catalytic reduction of cytochrome *c* (*41*). Only the D1393V mutation showed no significant difference between its nNOSr and nNOSfnr proteins. The NADPH oxidase activity of D1393N nNOSfnr was much higher than the corresponding activities of WT and D1393V nNOSfnr. This matches the results we obtained with the nNOSr proteins and indicates that reduced FAD species have an increased susceptibility to autooxidation in the D1393N mutant.

We measured the rate of FAD reduction of the nNOSfnr proteins by excess NADPH using stopped-flow spectrophotometry. Rapid-scan visible spectra collected during the reaction for each protein are given in Figure 4 along with single wavelength data at 458 nm (Figure 4, insets). The absorbance changes at 458 nm were fit to exponential functions as appropriate, and the calculated rate constants are given in Table 2. The most dramatic difference between the nNOSr and nNOSfnr proteins was seen in the D1393N mutant, where k_1 for the nNOSfnr protein was over 8 times larger than k_1 in the corresponding nNOSr. Each set of spectra obtained for each of the three nNOSfnr proteins had

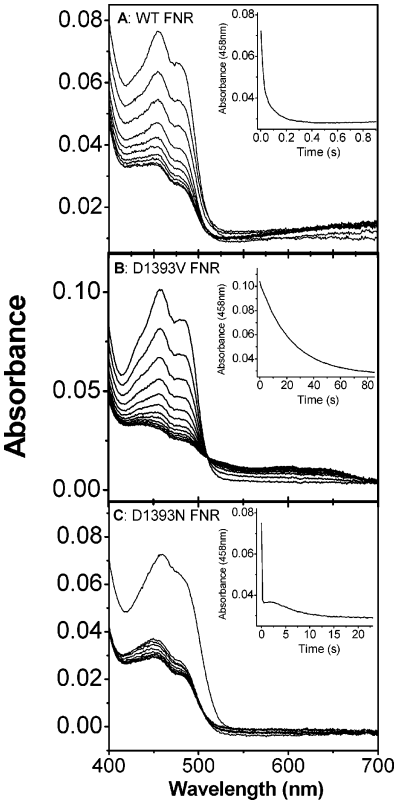

FIGURE 4: Stopped-flow data collected during the anaerobic flavin reduction of fully oxidized WT (panel A), D1393V (panel B), and D1393N (panel C) nNOSfnr by a 10-fold excess of NADPH at 10 °C. Each panel gives rapid-scan diode array spectra corresponding to a complete reduction reaction. The corresponding inset to each panel gives the single wavelength data collected at 458 nm associated with each set of diode-array spectra.

a distinct appearance. In the case of WT nNOSfnr (Figure 4, panel A), FAD reduction was accompanied by a broad increase in absorbance extending past 700 nm. This shows that the reduced WT nNOSfnr formed an $FADH_2-NADP^+$ charge-transfer complex after hyride transfer from NADPH, as previously observed in our WT nNOSr (*14*). The reduction of D1393V nNOSfnr (Figure 4, panel B) was characterized by a relatively slow gradual loss of absorbance at 458 nm and the simultaneous appearance of a broad absorbance band centered near 600 nm, characteristic of a flavin semiquinone. In this protein, hydride transfer to the FAD must be slow enough that there was sufficient time for oxidized and $FADH_2$ forms of the enzyme to disproportionate, yielding a significant population of the FAD semiquinone form. Finally, the reduction of D1393N nNOSfnr (Figure 4, panel C) was a unique triphasic process, which did not involve the formation of either semiquinone species or a charge−transfer complex.

Interaction of $NADP^+$ with nNOSr Proteins. Productive binding of $NADP^+$ to WT nNOSr and other FNR-like proteins causes a wavelength shift in their flavin absorbance properties most commonly characterized by a peak near 510 nm in the difference spectrum calculated using spectra collected before and after saturation with $NADP^+$ (*14*, *46*−*48*). Upon addition of $NADP^+$ to WT nNOSfnr, we observed changes in the absorbance spectrum (Figure 5, panel A) that were similar to those observed with WT nNOSr and human nNOSfnr (*14*, *39*), featuring a positive peak with a maximum value at 503 nm in the difference spectrum. No significant

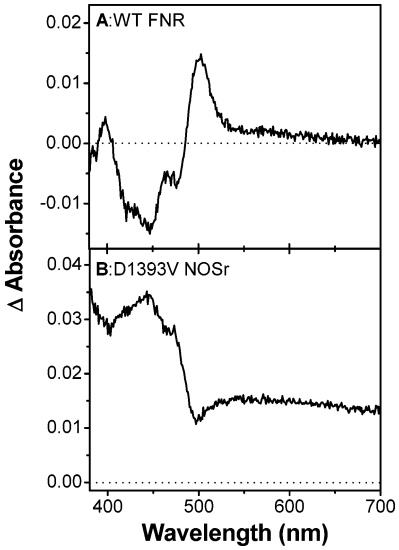

FIGURE 5: Spectral characterization of the interaction of $NADP^+$ with WT nNOSfnr (panel A) and D1393V nNOSr (panel B). The given difference spectra were calculated from fully oxidized $NADP^+$-free and $NADP^+$-saturated proteins to demonstrate visible spectral changes caused by the interaction between $NADP^+$ and the flavoproteins. The major peak observed in panel A has a maximum value at approximately 510 nm.

spectral changes were observed in D1393V nNOSfnr, D1393N nNOSfnr, and D1393N nNOSr, even in the presence of a large excess of $NADP^+$ (data not shown). However, saturation of D1393V nNOSr with $NADP^+$ did result in changes to its FAD absorption spectrum (Figure 5, panel B), although these changes were quite different from those seen in WT nNOSr or the nNOSfnr protein.

Thermodynamic Analysis of nNOSfnr Proteins. Redox titration of the FAD cofactor in our WT and mutant nNOSfnr proteins (Figure 6) showed that absorbance changes at 458 nm during the titrations fit to the two-electron Nernst equation (Figure 6, insets), from which we could estimate the equilibrium midpoint potentials (E_m) for two redox couples (oxidized/semiquinone, ox/sq; semiquinone/hydroquinone, sq/hq) in each protein. For WT nNOSfnr, the absorbance changes at 600 nm were also used to calculate E_m values in good agreement with those obtained at 458 nm, and we could then assign the individual 1-electron equilibrium redox potentials obtained (Table 4). The two E_m values determined for WT nNOSfnr are consistent with previous results (*49*). The amount of semiquinone buildup at 600 nm observed during the reduction of D1393V and D1393N nNOSfnr was so small that we could not obtain a meaningful fit of the data at this wavelength. Therefore, assignment of the individual 1-electron midpoint potentials in the mutant nNOSfnr proteins was not possible, and only the calculated 2-electron potentials are given in Table 4. The lack of semiquinone buildup in these mutants indicates that the mutation of D1393 had an affect on the FAD redox potentials involving decreased separation between the individual 1-electron E_m values.

Presteady-State Cytochrome c Reduction and the Role of Asp^{1393} in FMN Shielding. Electron transfer from nNOSr is regulated, at least in part, by an equilibrium between relatively shielded and deshielded (i.e., protein surface accessible) forms of the FMN cofactor bound within the FMN subdomain (*14*). In WT nNOSr, NADP(H) binding

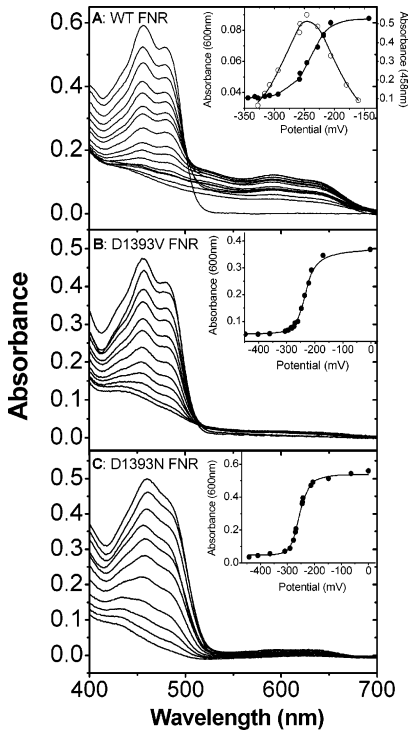

FIGURE 6: Potentiometric titrations of nNOSfnr proteins in 100 mM phosphate buffer at 25 °C. A representative set of visible spectra obtained during the potentiometric titration of each protein by dithionite/ferricyanide is given for WT nNOSfnr (panel A), D1393V nNOSfnr (panel B), and D1393N nNOSfnr (panel C). The inset to each panel contains a plot of absorbance at 458 nm (●) versus the electrochemical potential (mV) along with the best-fit line of the two-electron Nernst equation calculated as described in Experimental Procedures. Panel A, inset, also contains a plot of absorbance at 600 nm (○) versus the electrochemical potential (mV) along with a corresponding best-fit line of the two-electron Nernst equation for WT nNOSfnr. The equilibrium midpoint potentials (E_m) derived from these experiments are given in Table 4.

Table 4: Equilibrium Midpoint Potentials (E_m) vs SHE of nNOSfnr Proteins[a]

protein	E_m (ox/sq)	E_m (sq/hq)	E_m (2 e^- : ox/hq)
WT nNOSfnr	-214 ± 8 mV	-274 ± 9 mV	-244 mV
D1393V nNOSfnr	N/A	N/A	-228 mV
D1393N nNOSfnr	N/A	N/A	-265 mV

[a] The 1-electron equilibrium midpoint reduction potentials ((ox/sq), (sq/hq)) were determined for each protein by potentiometric titration as described under Experimental Procedures, and the 2-electron reduction potentials (ox/hq) were calculated on the basis of these results. Assignment of the 1-electron reduction potentials for the D1393 mutant proteins was not possible (see Results).

shifts the equilibrium toward a more FMN-shielded form, and CaM binding counteracts this effect resulting in a more FMN deshielded form. Accordingly, NADP(H) is an inhibitor of electron transfer from the FMN domain of WT nNOSr, and CaM binding is an activator. Measuring the rate of electron transfer between prereduced nNOSr and cytochrome *c* provides a way to compare relative amounts of FMN shielding under various experimental conditions (*13*, *14*). In order to determine whether or not Asp^{1393} has any role in the nNOSr internal regulatory system involving FMN shielding, we measured the rates (k_{obs}) of electron transfer between an excess of photoreduced nNOSr proteins and cytochrome *c* under various conditions in a stopped-flow spectrophotometer. The results, given in Figure 7, were calculated by

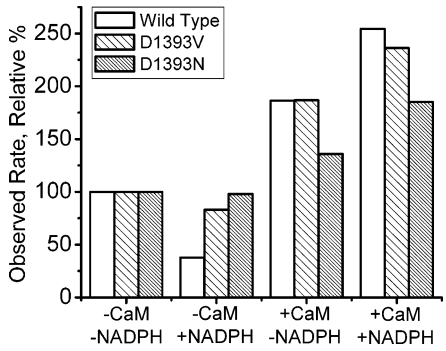

FIGURE 7: Summary of presteady-state cytochrome *c* reduction rates by prereduced WT, D1393V, and D1393N nNOSr proteins. The photoreduced proteins were rapidly mixed with a substoichiometric amount of cytochrome *c* in a stopped-flow instrument at 10 °C, and the absorbance changes at 550 nm were recorded and fit to a single-exponential function. The relative percent reduction rates were calculated and plotted for each protein as indicated to demonstrate the effects of CaM and NADPH binding on the electron transfer to cytochrome *c*.

fitting the absorbance changes recorded at 550 nm during the reaction to a first-order exponential function. In the absence of NADPH or CaM, we observed comparable k_{obs} values for WT, D1393V, and D1393N nNOSr (14 ± 0.1, 13.5 ± 0.2, and 19.5 ± 0.4, respectively). These values were set as the 100% values in Figure 7. Binding NADPH to WT nNOSr slowed its electron transfer to cytochrome *c*, as previously reported (*13*, *14*). The NADPH effect was less in D1393V nNOSr and did not occur at all in D1393N nNOSr. On the basis of these results, we conclude that Asp^{1393} is needed to cause an increase in FMN module shielding in NADPH-bound nNOSr. The mutation of Asp^{1393} did not have as much of an effect on FMN deshielding in response to CaM binding, although the CaM effect was reduced in the D1393N mutant (Figure 7). Thus, Asp^{1393} appears to be needed for nNOSr to properly change its FMN shielding in response to NADPH or CaM.

Effect of Asp^{1393} on the Rate of Interflavin Electron Transfer. Fully reduced nNOSr is capable of transferring up to three of its four electrons to cytochrome *c* (*13*). Electron transfer to cytochrome *c* always occurs from the FMN hydroquinone, and this step can occur very rapidly at sufficient cytochrome *c* concentrations. Following the first electron transfer between reduced nNOSr and excess cytochrome *c*, interflavin electron transfer must occur to regenerate $FMNH_2$ prior to any subsequent electron transfers. Therefore, the rate of reduction of cytochrome *c* after the first electron equivalent has been delivered from nNOSr provides an indicator of the rate of nNOSr interflavin electron transfer (*13*). We mixed photoreduced nNOSr proteins with a 10-fold excess of cytochrome *c* in the stopped-flow apparatus and the absorbance changes at 550 nm were recorded. The combined data are given in Figure 8. The initial absorbance point was approximated from experiments mixing only buffer with cytochrome *c*, and the data are plotted in terms of the change in absorbance from that point (designated as 0 on the *y* axis). The majority of the absorbance change captured took place within the first 1 to 2 s after mixing. The multiphasic absorbance curves fit well to a multiple exponential function yielding the rates (k_1-k_4) reported in Table 5. Under these conditions, at least the first electron transfer to cytochrome *c* took place in the instrument

Table 5: Rates of Oxidation of Reduced nNOSr Proteins by Excess Cytochrome *c*[a]

protein	k_1 (%)[b]	k_2 (%)	k_3 (%)	k_4 (%)
WT nNOSr	23 ± 0.3 (36)	3.6 ± 0.1 (20)	0.30 ± 0.003 (27)	0.03 ± 0.001 (17)
D1393V nNOSr	10 ± 0.3 (38)	2.2 ± 0.1 (20)	0.20 ± 0.001 (20)	0.04 ± 0.006 (22)
D1393N nNOSr	12 ± 0.5 (22)	2.6 ± 0.1 (20)	0.11 ± 0.009 (32)	0.09 ± 0.01 (26)

[a] Reactions were carried out in the stopped-flow instrument at 10 °C using an excess of cytochrome *c* while monitoring the absorbance changes at 550 nm. Data were fit to a multiple exponential function as described under Experimental Procedures. [b] Individual rate constants are reported as follows: calculated rate (s^{-1}) ± S.D. (% of the plotted curve corresponding to each particular kinetic phase).

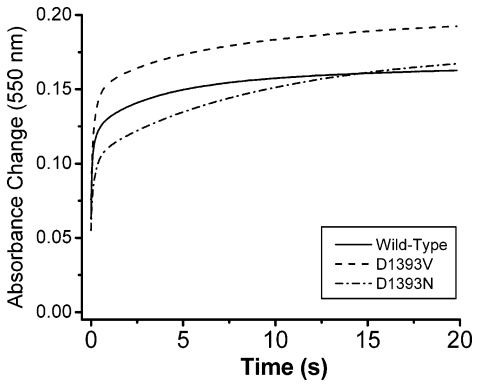

FIGURE 8: Oxidation of excess cytochrome *c* by prereduced WT (solid line), D1393V (dash line), and D1393N (dash-dot line) nNOSr proteins. The photoreduced proteins were rapidly mixed with a 10-fold excess of cytochrome *c* in a stopped-flow instrument at 10 °C, and the absorbance changes at 550 nm were recorded and fit to a multiple exponential function. The rate values obtained are reported in Table 5, and they provide an indication of the relative rates of interflavin electron transfer between the three proteins.

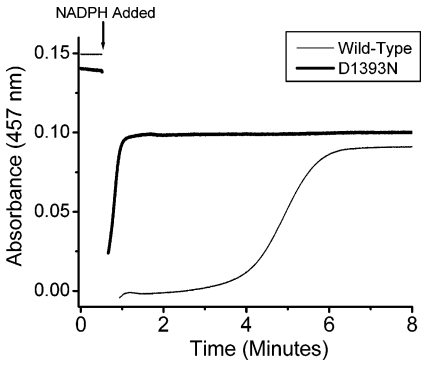

FIGURE 9: Autooxidation of NADPH-reduced WT nNOSr (thin line) and D1393N nNOSr (bold line). Each protein was treated with a 20-fold excess of NADPH in an air-saturated buffer at the point indicated and allowed to reoxidize at room temperature in the spectrophotometer while plotting the absorbance changes at 457 nm. On a longer time scale (>1 h), D1393N nNOSr returned to its original fully oxidized state while WT nNOSr remained in an air-stable semiquinone form (data not shown).

dead time (*13*). In each case, the plotted absorbance changes correspond to an additional 1.2−1.4 electron equivalents transferred to cytochrome *c*. Therefore, the absorbance traces captured and fit should be indicative of the rates of interflavin electron transfer, though we did not observe the full theoretical three electron equivalents possible. The differences among the three proteins with respect to the calculated rates (particularly the k_1 and k_2 values in Table 5) and the shapes of their corresponding absorbance curves suggest that the Asp[1393] mutants have somewhat slower interflavin electron-transfer rates relative to that of WT nNOSr.

Autooxidation of Reduced Flavins. Because of the large difference in NADPH oxidase activity between WT and D1393N nNOSr, we examined the stability of their reduced flavins under conditions that allowed autooxidation to take place. Both fully oxidized proteins were reduced with an excess (20-fold) of NADPH in an open cuvette containing air-saturated buffer, and the absorbance changes at 457 nm over time were recorded. The data are given in Figure 9. After the addition of NADPH, both proteins exhibited a significant loss of absorbance, as expected, due to flavin reduction. Almost immediately, the absorbance trace for D1393N nNOSr began to increase (k_{max} = 0.27 Abs/min), indicating that the NADPH had been consumed and that the flavins were undergoing reoxidation. In contrast, it took nearly 4 min for all of the NADPH to be consumed by WT nNOSr, and the subsequent rate of flavin oxidation (k_{max} = 0.051 Abs/min) was over 5-fold less than that for D1393N nNOSr. Both proteins achieved a similar final absorbance value in the experiment that was less than the initial absorbance value for the fully oxidized proteins. This indicates that they both returned to a more stable one-electron reduced state containing the FMN semiquinone. The results confirm that the D1393N mutant has a significantly increased susceptibility toward flavin autooxidation. An analogous experiment using D1393V nNOSr was not possible due to the extremely slow NADPH reduction of this protein.

DISCUSSION

In this study, we utilized the nNOSr and nNOSfnr proteins to investigate in detail the effects of Asp[1393] mutations on electron-transfer reactions, NADP(H) binding, FAD thermodynamics, and the regulatory system of nNOSr.

The mutation of Asp[1393] decreased cytochrome *c* reductase activities, mirroring what we observed previously in full-length nNOS (*34*) and consistent with the effect of mutating the corresponding amino acid in P450R (Asp[675]) (*50*). Although CaM binding resulted in a nearly 9-fold stimulation of cytochrome *c* reductase activity in WT nNOSr, the stimulation of the D1393V and D1393N mutants by CaM was 2.7- and 5.3-fold, respectively. This indicates that electron transfer in the mutants is either not fully repressed or not able to be de-repressed as much by CaM as in WT nNOSr. Such phenotypes may be due to a problem with the nNOSr internal regulatory system in the mutants, their inability to catalyze internal electron-transfer fast enough to reach higher turnover rates, or both. A third possibility is that NADPH-derived electrons are lost from the mutants to the environment via flavin oxidation in competition with reduction of cytochrome *c*.

In order to understand how these mutations actually result in the observed phenotypes, we first studied the anaerobic reaction between fully oxidized flavoprotein and excess NADPH by stopped-flow spectroscopy. The calculated rates for the multiple phases of flavin reduction in the D1393V

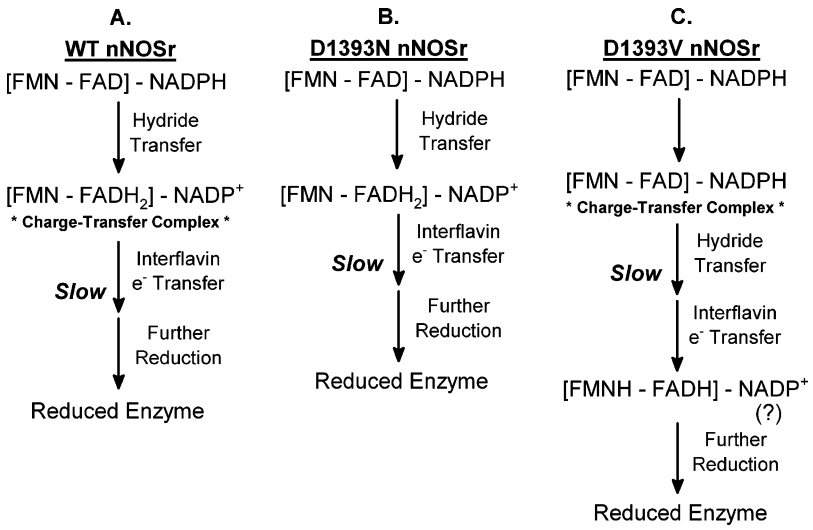

FIGURE 10: Summary of the spectral intermediates observed and the apparent sequence of reduction and interflavin (FAD → FMN) electron-transfer events occurring during the anaerobic reduction of fully oxidized WT nNOSr (A), D1393N nNOSr (B), and D1393V nNOSr (C) by a 10-fold excess of NADPH. For each protein, the slowest kinetic phase occurring during the reduction process, as determined by analysis of the collective stopped-flow data, is indicated.

and D1393N nNOSr mutants (Tables 2 and 3) were slower than the corresponding rates measured in WT nNOSr, with the rate of reduction of the D1393V mutant being dramatically inhibited. This again parallels the results obtained with comparable mutants of full-length nNOS and P450R (*34*, *50*). These similarities indicate that there is overlap of the functions of nNOS Asp^{1393} and P450R Asp^{675}.

The spectral data enable us to describe the intermediates appearing in each nNOSr protein during reduction by NADPH and identify the steps that occur during the reactions. Interestingly, the data indicate that the rate-limiting step can differ for each protein. The reduction of WT nNOSr (Figure 10A) begins with hydride transfer to FAD and the buildup of an $FADH_2-NADP^+$ charge-transfer complex as the first spectral intermediate (*14*). Interflavin electron transfer (possibly triggered by $NADP^+$ release) (*13*, *14*) and further reduction of the protein by additional NADPH equivalents follow, and these events are associated with decay of the $FADH_2-NADP^+$ charge-transfer spectrum. The buildup of the $FADH_2-NADP^+$ charge-transfer complex and the lack of a significant flavin semiquinone buildup during this reaction implies that the relatively slow step in the reduction process of WT nNOSr is interflavin electron transfer.

Neither of the two mutants examined in this study behaved exactly like WT nNOSr during reduction with respect to the sequence of spectral intermediates observed. The D1393N mutant (Figure 10B), however, was quite similar. The only notable difference between the two was that the initial phase of the reduction of D1393N nNOSr involved relatively fast hydride transfer to FAD without the corresponding formation of an $FADH_2-NADP^+$ charge-transfer complex. It was only during the second, slower, phase involving interflavin electron-transfer that any evidence of a charge-transfer complex was seen in D1393N nNOSr, and this occurred along with evidence of flavin semiquinone buildup. Thus, in D1393N nNOSr, the slow step during flavin reduction appears to be interflavin electron transfer, and the faster phase involves hydride transfer. The behavior of WT nNOSfnr and D1393N nNOSfnr during reduction by NADPH is consistent with what we observed for the corresponding nNOSr proteins. Hydride transfer to WT nNOSfnr yielded a $FADH_2-NADP^+$ charge-transfer complex, but hydride transfer to D1393N nNOSfnr did not. We suspect that orientation between the NADPH nicotinamide and the FAD cofactor in the D1393N mutant may be altered in a such a way as to prevent the formation of this charge-transfer complex (see below).

The spectral intermediates and relative rates during flavin reduction are completely different in D1393V nNOSr (Figure 10C). NADPH first binds to form a charge-transfer complex between oxidized FAD and NADPH, something not observed in the other proteins. In the next step, we expect hydride transfer to occur with appearance of an $FADH_2$/FMNox species, but the spectral changes and isosbestic point we observed during the reaction indicate instead that the NADPH-bound enzyme converts from a fully oxidized form into a disemiquinone form. Given that this requires two distinct consecutive steps (hydride transfer and then interflavin electron transfer), the data can only be explained by a slow hydride transfer from NADPH followed by a relatively fast FAD-to-FMN interflavin transfer in D1393V nNOSr. Thus, hydride transfer is the slow step that limits flavin reduction in this mutant. The buildup of the flavin semiquinone species reached a maximum level at the end of the first kinetic phase, approximately 100 s after initiating the reaction. After that point, hydride transfer from a second molecule of NADPH reduced the enzyme further until the protein reached a stable thermodynamic equilibrium of 3- and 4-electron-reduced forms. Overall, these differences between WT nNOSr and the D1393V/N mutants reinforce the concept that Asp^{1393} is important in the NADPH-dependent reduction of nNOSr.

It is possible that the slower hydride transfer to FAD as well as the different appearance and nature of the charge-transfer complexes formed during reduction by NADPH reflect an altered NADPH/$NADP^+$ nicotinamide binding orientation in the Asp^{1393} mutant enzymes. This follows from crystal structures of the related enzymes P450R and FNR, which show that the side chain carboxylate of their analogous

acidic residues can form a hydrogen bond with the nicotinamide ring of NADPH that positions it against the FAD ring system when bound in the productive conformation. This conformation is referred to as productive because it enables hydride transfer between NADPH and FAD. Productive binding of $NADP^+$ to oxidized flavoprotein often results in a shift in the flavin (FAD) absorbance spectra (*14*, *39*, *46*−*48*). Although we observed the characteristic spectral changes associated with productive $NADP^+$ binding in the WT nNOSr and nNOSfnr enzymes, they were not generally observed in any of the Asp^{1393} mutant enzymes. Only D1393V nNOSr yielded a significant difference spectrum upon saturation with $NADP^+$ (Figure 5B), but this spectrum was unlike the ones obtained using WT proteins. Interestingly, the analogous mutant G301A in *Anabaena* PCC 7119 FNR exhibited flavin absorbance shifts similar to those of the WT FNR enzyme after $NADP^+$ binding (*51*). However, mutations of Glu^{312} in spinach FNR do alter the flavin absorbance shifts upon saturation with $NADP^+$ compared to those in WT enzyme (*52*). Our results suggest that Asp^{1393} mutations, which change or eliminate the potential of the Asp carboxylate to form a hydrogen bond, have an effect on the nicotinamide−FAD interaction in nNOSr. This may result in the observed compromised hydride transfer reactions. Furthermore, this seems likely to be a specific effect of the point mutation at Asp^{1393}, because the mutation of neighboring Phe^{1395} had no influence on the characteristics of the absorbance shift induced by productive $NADP^+$ binding in nNOSr (*14*).

Our spectroelectrochemical titrations with nNOSfnr proteins showed that the D1393V and D1393N mutations altered the FAD midpoint equilibrium redox potentials. Changes in FAD redox potential were also found in mutations of the corresponding acidic residues in P450R and FNR (*50*, *52*). The effect of the Asp^{1393} mutations on FAD thermodynamics explains characteristics of the visible spectra we observed during the reductive titration of our nNOSfnr proteins. Stepwise reduction of WT nNOSfnr with dithionite resulted in a significant buildup of the FAD semiquinone species prior to the formation of the FAD hydroquinone during the addition of a second electron equivalent (Figure 6, panel A). Such behavior is consistent with a relatively large separation between the FAD E_m (ox/sq) and E_m (sq/hq) values for the protein-bound cofactor. The amount of semiquinone buildup observed during the reduction of the mutant nNOSfnr proteins (Figure 6, panels B, C) was practically negligible, indicating that the separation (in mV) between the 1-electron E_m values of D1393V and D1393N nNOSfnr has changed significantly relative to that of WT nNOSfnr. Because of this fact, we could only reliably report the calculated 2-electron E_m (ox/hq) value for the mutants. The small amount of change at 600 nm during the titrations implies that our D1393 nNOSfnr mutants have destabilized FAD semiquinones. In the extreme case, the 1-electron E_m values could even cross over each other, increasing the likelihood that the FAD cofactors in these proteins could participate in 2-electron reductions. A destabilized semiquinone would increase the barrier to FAD−FMN single electron transfer in our D1393V and D1393N nNOSr proteins and perhaps be a factor in the lower observed cytochrome *c* reductase activities of the mutants. The rate of FAD reduction by hydride transfer in D1393V nNOSr, as approximated by k_1 in Table 2, is about 1000 times slower than that in WT nNOSr. This must be due to an effect of Asp^{1393} not involving flavin thermodynamics because the calculated midpoint potential for the oxidized/2-electron reduced FAD couple in D1393V nNOSr (Table 4) is actually more positive than the corresponding value in WT nNOSr, a trend that should favor, not inhibit, hydride transfer from the low-potential NADPH to FAD. Because of the dramatically lowered rate of hydride transfer to D1393V nNOSr, it is not likely that thermodynamic effects involving interflavin electron-transfer play a significant role in the catalytic phenotype of this enzyme. The situation in D1393N nNOSr is more complex, and altered FAD thermodynamics, in addition to the factors discussed below, may be involved. However, we indirectly compared the relative rates of interflavin electron transfer in our nNOSr proteins by observing their reduction of excess cytochrome *c* (Figure 8; Table 5). These data indicate only a modest drop in the rate of interflavin electron transfer in either mutant compared to that in WT nNOSr, a fact which does not seem to strongly support the idea of a significantly increased barrier to FAD semiquinone formation during interflavin single electron transfer in these mutants.

The nNOSr flavoprotein contains a unique regulatory system controlling the rate of reduction of NOS heme and other electron acceptors. Part of the control involves a mechanism that alters the position of an equilibrium between relatively shielded and deshielded forms of the FMN cofactor (*13*, *14*). In WT nNOSr, binding NADPH inhibits electron transfer by stabilizing a more FMN-shielded form of the protein, whereas binding CaM counteracts this effect and deshields the FMN to stimulate electron transfer (*13*, *14*, *30*). Although the D1393V mutation had the greatest affect on flavin reduction kinetics and steady-state activities, the FMN shielding mechanism was most affected by the D1393N mutation (Figure 7). In this mutant, binding NADPH had virtually no effect on the FMN shielding compared to that in the NADPH-free enzyme. Binding CaM to D1393N nNOSr deshielded the FMN, but the amount of deshielding was less than that observed in both WT and D1393V nNOSr. Based strictly on these results, one might expect that the amount of stimulation of steady-state cytochrome *c* reduction by CaM binding should decrease in the order WT nNOSr > D1393V nNOSr > D1393N nNOSr. However, this was not the case because CaM stimulated cytochrome *c* reductase activity in D1393N nNOSr more than in D1393V nNOSr (Table 1). This discrepancy is potentially explained by considering the cytochrome *c* reductase activities of our nNOSfnr proteins. Although the activities of WT and D1393N nNOSfnr were, as expected, much less than the values found with the corresponding nNOSr proteins, the steady-state cytochrome *c* reductase activities of D1393V nNOSr and nNOSfnr were similar. Thus, the D1393V nNOSr mutant may represent an unusual case where the rate of hydride transfer from NADPH is inhibited so significantly that the reduction of cytochrome *c* via the FAD cofactor becomes a viable pathway. When electrons can be transferred via the FAD, the effect of CaM on FMN shielding, as judged by steady-state cytochrome *c* reductase activity, is reduced. Furthermore, the 2.7-fold stimulation of cytochrome *c* reduction by CaM that was observed in D1393V nNOSr (Table 1) could represent the portion of reduction that takes place via the FMN cofactor due to its becoming deshielded

by CaM. Earlier studies measuring flavin fluorescence in full-length nNOS Asp^{1393} mutants suggested that CaM binding induced normal protein conformational effects (*34*). It is now clear from these more detailed experiments using nNOSr proteins that the presence of Asp^{1393} in nNOS is required for normal behavior of the conformational regulatory system, particularly in response to NADPH. However, it is uncertain if there is a specific role for Asp^{1393} with regard to regulation or if the effects observed in this study are simply due to its proximity to Phe^{1395}, a conserved FAD-stacking amino acid that is required for the FMN shielding effect upon NADPH binding (*14*).

On the basis of our results, it is clear that the low steady-state cytochrome *c* reductase activity of D1393V nNOSr relative to that of WT nNOSr is primarily, if not exclusively, due to its extremely slow rate of hydride transfer from NADPH. This also appears to play a role in the lack of stimulation of this activity by CaM (see above). The situation with regard to D1393N nNOSr is more complex. In the CaM-free enzyme, there is almost no FMN shielding caused by NADPH binding. Thus, the FMN cofactor in CaM-free, NADPH-bound D1393N nNOSr is less shielded on average than that in the corresponding WT nNOSr. Despite this, the steady-state cytochrome *c* reductase activity of the CaM-free mutant is lower. Because the difference between the two enzymes cannot be due simply to FMN shielding, the lower activity of the mutant must be due to a compromised ability of the D1393N enzyme to form the $FMNH_2$ species to deliver electrons to cytochrome *c*. During steady-state NADPH oxidation, the flavins of full-length WT nNOS exist in an almost completely reduced state, whereas the flavins in full-length D1393N nNOS exist in a half-oxidized state (*34*). We had previously interpreted this as evidence of compromised interflavin electron transfer in D1393N nNOS (*34*). However, our current findings suggest that interflavin electron-transfer rates in WT and D1393N nNOSr are within a factor of 2 (Figure 8, Tables 1 and 5), which is not enough to fully explain the observed differences in catalytic activity based on the knowledge that interflavin electron transfer is the slow step for flavin reduction in D1393N nNOSr. Finally, we can consider the steady-state NADPH oxidase activity (Table 1) and roles for flavin autooxidation (Figure 9). Steady-state NADPH oxidation is the only catalytic activity for which the D1393N mutant has a higher value than that in WT nNOSr. This also holds for the D1393N nNOSfnr protein, whose NADPH oxidase activity is 7 times higher than that in WT nNOSfnr. Consistent with this, flavin autooxidation in D1393N nNOSr is much faster than that in WT nNOSr. These data indicate that the D1393N mutation significantly enhances electron loss from the reduced flavoprotein to O_2. Moreover, because the NADPH oxidase activity of D1393N nNOSr is comparable to its cytochrome *c* reductase activity, the loss of electrons via air oxidation should be competitive with cytochrome *c* reduction in this mutant in an air-saturated buffer. To test this possibility, we measured the cytochrome *c* reductase activity of CaM-free D1393N nNOSr under conditions with at least 80% less oxygen in the buffer, and we observed an approximately 60% increase in the measured activity, lending strong support for this concept. Thus, uncoupled electron-transfer due to increased flavin autooxidation contributes to the low cytochrome *c* reductase activity of D1393N nNOSr. This effect, along with an inhibited interflavin electron-transfer due to destabilization of the FAD semiquinone, may also explain why the flavins are in a half-oxidized state during steady-state NADPH oxidation by CaM-bound full-length D1393N nNOS (*34*).

Asp^{1393} is part of a conserved catalytic triad that is known to facilitate hydride transfer between NADPH and FAD in related flavoproteins (*6*, *31*−*34*). Within the catalytic triad, proposals for the function of the acidic residue include proton donation to the FAD, proper positioning of the NADPH nicotinamide against the FAD isoalloxazine ring for hydride transfer, and modulation of FAD reduction potentials. In the case of nNOS, its proximity to the *C*-terminal tail also suggests that it could be involved in the unique conformational regulatory system. These functional roles may be achieved by the Asp^{1393} side chain acting as an acid or base, being involved in hydrogen bonding, or using its negative charge to influence FAD redox potentials through electrostatic interactions. In the context of our D1393V and D1393N nNOSr mutants, the Val side chain cannot substitute well for Asp in any of these roles, consistent with the dramatic effect of this substitution on nNOSr properties. Although the acid−base properties of Asn and Asp differ considerably, the flavin reduction rate associated with hydride transfer in D1393N nNOSr was only 10-fold slower than that in WT nNOSr. Therefore, acting as a proton donor or acceptor is not likely to be the primary role for Asp^{1393} in hydride transfer to FAD. A similar conclusion was achieved regarding the role of Glu^{312} in spinach FNR (*52*). However, because the Asn side chain can function as a hydrogen bond donor or acceptor and the Val side chain cannot, our results suggest that hydrogen bonding is an important role of Asp^{1393} in the hydride transfer reaction. Specifically, existing structural information indicates that hydrogen bonding is required for optimal positioning of the NADPH nicotinamide near the FAD (*6*, *31*−*33*). It follows that the lack of hydrogen bonding and steric bulk of the Val side chain would alter the interaction between the nicotinamide and FAD more significantly than the conservative Asp/Asn exchange and result in greater inhibition of hydride transfer as observed in D1393V nNOSr. Finally, we observed changes in FAD potentials that suggest the negative charge of Asp^{1393} has a role in modulating FAD thermodynamic properties, similar to the function of Glu^{312} in spinach FNR (*52*).

An important finding of this study is the high rate of flavin oxidation and steady-state NADPH oxidation by D1393N nNOSr and nNOSfnr. It appears that the loss of electron equivalents to O_2 is an important reason for the lower cytochrome *c* reductase activity of this enzyme compared to that of WT nNOSr. A comparison of the two constructs (D1393N nNOSr and nNOSfnr, Table 1) reveals that a significant portion of electrons are lost from the FAD. The reaction of reduced flavins and flavoproteins with O_2 can occur via multiple pathways (*53*). Interestingly, the mutation of Glu^{301} in *Anabaena* PCC 7119 FNR to Ala resulted in a change in the mechanism of FAD oxidation by O_2 (*51*, *54*). One result was a nearly 4-fold increase in its NADPH oxidase activity (*51*). Generally, reduced FNR reacts with molecular oxygen to yield superoxide plus a thermodynamically stabilized FAD semiquinone (*55*). A mutation that allows easier access of oxygen to the reduced flavin could result in a faster flavin oxidation by this mechanism. An alternative

pathway, likely to be occurring in the G301A mutant of *Anabaena* PCC 7119 FNR (*51*, *54*), involves an FAD 4a-hydroperoxide intermediate and leads to the formation of H_2O_2 instead of superoxide and no formation of a stable flavin semiquinone. In order for the second pathway to become viable, there must be sufficient space surrounding the flavin to accommodate the 4a-hydroperoxide intermediate. The existence of such space in G301A *Anabaena* PCC 7119 FNR was confirmed by structural studies and modeling (*54*). In D1393N nNOSr, the mutated residue (Asn) is nearly identical in size to the one it replaced (Asp). Thus, it is reasonable to assume that the steric environments around the FAD in WT nNOSr and D1393N nNOSr are similar, making the difference in NADPH oxidase activities between the two enzymes more surprising. Further studies to probe the flavin oxidation kinetics, oxidation product identification, and structural work to explore the possibility of an unexpected protein rearrangement would help to characterize the reaction between reduced D1393N nNOSr and O_2 in more detail. Additional data would also help to understand the broader functions of the catalytic triad in the flavoprotein domain of nNOS.

ACKNOWLEDGMENT

We thank Dr. Marian Stankovich for advice and helpful discussions regarding the flavin potentiometric titrations, Dr. Sandro Ghisla for help in identifying the 6-hydroxy FAD cofactor, Mauro Tiso for assistance with the preparation and characterization of nNOSfnr proteins, and Deborah Durra for assistance with protein preparation and characterization.

REFERENCES

1. Furchgott, R. F. (1999) Endothelium-derived relaxing factor: Discovery, early studies, and identification as nitric oxide, *Biosci. Rep. 19*, 235−251.
2. Ignarro, L. J. E. (2000) *Nitric Oxide: Biology and Pathobiology*, Academic Press, San Diego, CA.
3. Marletta, M. A., Hurshman, A. R., and Rusche, K. M. (1998) Catalysis by nitric oxide synthase, *Curr. Opin. Chem. Biol. 2*, 656−663.
4. Stuehr, D. J. (1999) Mammalian nitric oxide synthases, *Biochim. Biophys. Acta 1411*, 217−230.
5. Wei, C. C., Crane, B. R., and Stuehr, D. J. (2003) Tetrahydrobiopterin radical enzymology, *Chem. Rev. 103*, 2365−2383.
6. Wang, M., Roberts, D. L., Paschke, R., Shea, T. M., Masters, B. S. S., and Kim, J. J. P. (1997) Three-dimensional structure of NADPH-cytochrome P450 reductase: Prototype for FMN- and FAD-containing enzymes, *Proc. Natl. Acad. Sci. U.S.A. 94*, 8411−8416.
7. Bredt, D. S., Hwang, P. M., Glatt, C. E., Lowenstein, C., Reed, R. R., and Snyder, S. H. (1991) Cloned and expressed nitric-oxide synthase structurally resembles cytochrome-P-450 reductase, *Nature 351*, 714−718.
8. Olteanu, H., and Banerjee, R. (2001) Human methionine synthase reductase, a soluble P-450 reductase-like dual flavoprotein, is sufficient for NADPH-dependent methionine synthase activation, *J. Biol. Chem. 276*, 35558−35563.
9. Paine, M. J. I., Garner, A. P., Powell, D., Sibbald, J., Sales, M., Pratt, N., Smith, T., Tew, D. G., and Wolf, C. R. (2000) Cloning and characterization of a novel human dual flavin reductase, *J. Biol. Chem. 275*, 1471−1478.
10. Karplus, P. A., Daniels, M. J., and Herriott, J. R. (1991) Atomic-structure of ferredoxin-NADP$^+$ reductase: prototype for a structurally novel flavoenzyme family, *Science. 251*, 60−66.
11. Watenpaugh, K. D., Sieker, L. C., and Jensen, L. H. (1973) The binding of riboflavin-5′-phosphate in a flavoprotein: Flavodoxin at 2.0- angstrom resolution, *Proc. Natl. Acad. Sci. U.S.A. 70*, 3857−3860.
12. Finn, R. D., Basran, J., Roitel, O., Wolf, C. R., Munro, A. W., Paine, M. J. I., and Scrutton, N. S. (2003) Determination of the redox potentials and electron transfer properties of the FAD- and FMN-binding domains of the human oxidoreductase NR1, *Eur. J. Biochem. 270*, 1164−1175.
13. Craig, D. H., Chapman, S. K., and Daff, S. (2002) Calmodulin activates electron transfer through neuronal nitric-oxide synthase reductase domain by releasing an NADPH-dependent conformational lock, *J. Biol. Chem. 277*, 33987−33994.
14. Konas, D. W., Zhu, K., Sharma, M., Aulak, K. S., Brudvig, G. W., and Stuehr, D. J. (2004) The FAD-shielding residue Phe-(1395) regulates neuronal nitric-oxide synthase catalysis by controlling NADP(+) affinity and a conformational equilibrium within the flavoprotein domain, *J. Biol. Chem. 279*, 35412−35425.
15. Salerno, J. C., Harris, D. E., Irizarry, K., Patel, B., Morales, A. J., Smith, S. M. E., Martasek, P., Roman, L. J., Masters, B. S. S., Jones, C. L., Weissman, B. A., Lane, P., Liu, Q., and Gross, S. S. (1997) An autoinhibitory control element defines calcium-regulated isoforms of nitric oxide synthase, *J. Biol. Chem. 272*, 29769−29777.
16. Daff, S., Sagami, I., and Shimizu, T. (1999) The 42-amino acid insert in the FMN domain of neuronal nitric-oxide synthase exerts control over Ca2+/calmodulin-dependent electron transfer, *J. Biol. Chem. 274*, 30589−30595.
17. Lane, P., and Gross, S. S. (2000) The autoinhibitory control element and calmodulin conspire to provide physiological modulation of endothelial and neuronal nitric oxide synthase activity, *Acta Physiol. Scand. 168*, 53−63.
18. Montgomery, H. J., Romanov, V., and Guillemette, J. G. (2000) Removal of a putative inhibitory element reduces the calcium-dependent calmodulin activation of neuronal nitric-oxide synthase, *J. Biol. Chem. 275*, 5052−5058.
19. Roman, L. J., Martasek, P., Miller, R. T., Harris, D. E., de la Garza, M. A., Shea, T. M., Kim, J. J. P., and Masters, B. S. S. (2000) The C termini of constitutive nitric-oxide synthases control electron flow through the flavin and heme domains and affect modulation by calmodulin, *J. Biol. Chem. 275*, 29225−29232.
20. Roman, L. J., Miller, R. T., de la Garza, M. A., Kim, J. J. P., and Masters, B. S. S. (2000) The C terminus of mouse macrophage inducible nitric-oxide synthase attenuates electron flow through the flavin domain, *J. Biol. Chem. 275*, 21914−21919.
21. Lane, P., and Gross, S. S. (2002) Disabling a C-terminal autoinhibitory control element in endothelial nitric-oxide synthase by phosphorylation provides a molecular explanation for activation of vascular NO synthesis by diverse physiological stimuli, *J. Biol. Chem. 277*, 19087−19094.
22. Fulton, D., Gratton, J. P., Mccabe, T. J., Fontana, J., Fujio, Y., Walsh, K., Franke, T. F., Papapetropoulos, A., and Sessa, W. C. (1999) Regulation of endothelium-derived nitric oxide production by the protein kinase Akt, *Nature 400*, 792.
23. Hayashi, Y., Nishio, M., Naito, Y., Yokokura, H., Nimura, Y., Hidaka, H., and Watanabe, Y. (1999) Regulation of neuronal nitric-oxide synthase by calmodulin kinases, *J. Biol. Chem. 274*, 20597−20602.
24. Dimmeler, S., Fleming, I., Fisslthaler, B., Hermann, C., Busse, R., and Zeiher, A. M. (1999) Activation of nitric oxide synthase in endothelial cells by Akt-dependent phosphorylation, *Nature 399*, 601−605.
25. Chen, Z. P., Mitchelhill, K. I., Michell, B. J., Stapleton, D., Rodriguez-Crespo, I., Witters, L. A., Power, D. A., de Montellano, P. R. O., and Kemp, B. E. (1999) AMP-activated protein kinase phosphorylation of endothelial NO synthase, *FEBS Lett. 443*, 285−289.
26. Butt, E., Bernhardt, M., Smolenski, A., Kotsonis, P., Frohlich, L. G., Sickmann, A., Meyer, H. E., Lohmann, S. M., and Schmidt, H. H. H. W. (2000) Endothelial nitric-oxide synthase (type III) is activated and becomes calcium independent upon phosphorylation by cyclic nucleotide-dependent protein kinases, *J. Biol. Chem. 275*, 5179−5187.
27. Adak, S., Santolini, J., Tikunova, S., Wang, Q., Johnson, J. D., and Stuehr, D. J. (2001) Neuronal nitric-oxide synthase mutant (Ser-1412 → Asp) demonstrates surprising connections between heme reduction, NO complex formation, and catalysis, *J. Biol. Chem. 276*, 1244−1252.
28. Knudsen, G. M., Nishida, C. R., Mooney, S. D., and de Montellano, P. R. O. (2003) Nitric-oxide synthase (NOS) reductase domain models suggest a new control element in endothelial NOS that attenuates calmodulin-dependent activity, *J. Biol. Chem. 278*, 31814−31824.

29. Adak, S., Sharma, M., Meade, A. L., and Stuehr, D. J. (2002) A conserved flavin-shielding residue regulates NO synthase electron transfer and nicotinamide coenzyme specificity, *Proc. Natl. Acad. Sci. U.S.A. 99*, 13516−13521.
30. Tiso, M., Konas, D. W., Panda, K., Garcin, E. D., Sharma, M., Getzoff, E. D., and Stuehr, D. J. (2005) C-terminal tail residue Arg(1400) enables NADPH to regulate electron transfer in neuronal nitric-oxide synthase, *J. Biol. Chem. 280*, 39208−39219.
31. Zhang, J., Martasek, P., Paschke, R., Shea, T., Masters, B. S. S., and Kim, J. J. P. (2001) Crystal structure of the FAD/NADPH-binding domain of rat neuronal nitric-oxide synthase: Comparisons with NADPH-cytochrome P450 oxidoreductase, *J. Biol. Chem. 276*, 37506−37513.
32. Kurisu, G., Kusunoki, M., Katoh, E., Yamazaki, T., Teshima, K., Onda, Y., Kimata-Ariga, Y., and Hase, T. (2001) Structure of the electron transfer complex between ferredoxin and ferredoxin-NADP(+) reductase, *Nat. Struct. Biol. 8*, 117−121.
33. Garcin, E. D., Bruns, C. M., Lloyd, S. J., Hosfield, D. J., Tiso, M., Gachhui, R., Stuehr, D. J., Tainer, J. A., and Getzoff, E. D. (2004) Structural basis for isozyme-specific regulation of electron transfer in nitric-oxide synthase, *J. Biol. Chem. 279*, 37918−37927.
34. Panda, K., Adak, S., Konas, D., Sharma, M., and Stuehr, D. J. (2004) A conserved aspartate (Asp-1393) regulates NADPH reduction of neuronal nitric-oxide synthase: Implications for catalysis, *J. Biol. Chem. 279*, 18323−18333.
35. Gachhui, R., Presta, A., Bentley, D. F., AbuSoud, H. M., McArthur, R., Brudvig, G., Ghosh, D. K., and Stuehr, D. J. (1996) Characterization of the reductase domain of rat neuronal nitric oxide synthase generated in the methylotrophic yeast Pichia pastoris: Calmodulin response is complete within the reductase domain itself, *J. Biol. Chem. 271*, 20594−20602.
36. Matsuda, H., and Iyanagi, T. (1999) Calmodulin activates intramolecular electron transfer between the two flavins of neuronal nitric oxide synthase flavin domain, *Biochim. Biophys. Acta 1473*, 345−355.
37. Knight, K., and Scrutton, N. S. (2002) Stopped-flow kinetic studies of electron transfer in the reductase domain of neuronal nitric oxide synthase: Re-evaluation of the kinetic mechanism reveals new enzyme intermediates and variation with cytochrome P450 reductase, *Biochem. J. 367*, 19−30.
38. Guan, Z. W., Kamatani, D., Kimura, S., and Iyanagi, T. (2003) Mechanistic studies on the intramolecular one-electron transfer between the two flavins in the human neuronal nitric-oxide synthase and inducible nitric-oxide synthase flavin domains, *J. Biol. Chem. 278*, 30859−30868.
39. Guan, Z. W., and Iyanagi, T. (2003) Electron transfer is activated by calmodulin in the flavin domain of human neuronal nitric oxide synthase, *Arch. Biochem. Biophys. 412*, 65−76.
40. Garnaud, P. E., Koetsier, M., Ost, T. W. B., and Daff, S. (2004) Redox properties of the isolated flavin mononucleotide- and flavin adenine dinucleotide-binding domains of neuronal nitric oxide synthase, *Biochemistry 43*, 11035−11044.
41. Adak, S., Ghosh, S., Abu-Soud, H. M., and Stuehr, D. J. (1999) Role of reductase domain cluster 1 acidic residues in neuronal nitric-oxide synthase: Characterization of the FMN-free enzyme, *J. Biol. Chem. 274*, 22313−22320.
42. Stankovich, M. T. (1980) An anaerobic spectroelectrochemical cell for studying the spectral and redox properties of flavoproteins, *Anal. Biochem. 109*, 295−308.
43. Ermler, U., Ghisla, S., Massey, V., and Schulz, G. E. (1991) Structural, spectroscopic and catalytic activity studies on glutathione-reductase reconstituted with fad analogs, *Eur. J. Biochem. 199*, 133−138.
44. Marshall, K. R., Gong, M., Wodke, L., Lamb, J. H., Jones, D. J. L., Farmer, P. B., Scrutton, N. S., and Munro, A. W. (2005) The human apoptosis-inducing protein AMID is an oxidoreductase with a modified flavin cofactor and DNA binding activity, *J. Biol. Chem. 280*, 30735−30740.
45. Massey, V., and Palmer, G. (1962) Charge transfer complexes of lipoyl dehydrogenase and free flavins, *J. Biol. Chem. 237*, 2347−2358.
46. Deng, Z., Aliverti, A., Zanetti, G., Arakaki, A., Ottado, J., Orellano, E. G., Calcaterra, N. B., Ceccarelli, E. A., Carrilli, N., and Karplus, P. A. (1999) A productive NADP(+) binding mode of ferredoxin-NADP(+) reductase revealed by protein engineering and crystallographic studies, *Nat. Struct. Biol. 6*, 847−853.
47. Piubelli, L., Aliverti, A., Arakaki, A. K., Carrillo, N., Ceccarelli, E. A., Karplus, P. A., and Zanetti, G. (2000) Competition between C-terminal tyrosine and nicotinamide modulates pyridine nucleotide affinity and specificity in plant ferredoxin-NADP(+) reductase, *J. Biol. Chem. 275*, 10472−10476.
48. Hubbard, P. A., Shen, A. L., Paschke, R., Kasper, C. B., and Kim, J. J. P. (2001) NADPH-cytochrome P450 oxidoreductase: Structural basis for hydride and electron transfer, *J. Biol. Chem. 276*, 29163−29170.
49. Noble, M. A., Munro, A. W., Rivers, S. L., Robledo, L., Daff, S. N., Yellowlees, L. J., Shimizu, T., Sagami, I., Guillemette, J. G., and Chapman, S. K. (1999) Potentiometric analysis of the flavin cofactors of neuronal nitric oxide synthase, *Biochemistry 38*, 16413−16418.
50. Shen, A. L., Sem, D. S., and Kasper, C. B. (1999) Mechanistic studies on the reductive half-reaction of NADPH-cytochrome P450 oxidoreductase, *J. Biol. Chem. 274*, 5391−5398.
51. Medina, M., Martinez-Julvez, M., Hurley, J. K., Tollin, G., and Gomez-Moreno, C. (1998) Involvement of glutamic acid 301 in the catalytic mechanism of ferredoxin-NADP(+) reductase from Anabaena PCC 7119, *Biochemistry 37*, 2715−2728.
52. Aliverti, A., Deng, Z., Ravasi, D., Piubelli, L., Karplus, P. A., and Zanetti, G. (1998) Probing the function of the invariant glutamyl residue 312 in spinach ferredoxin-NADP(+) reductase, *J. Biol. Chem. 273*, 34008−34015.
53. Ghisla, S., and Massey, V. (1989) Mechanisms of flavoprotein-catalyzed reactions, *Eur. J. Biochem. 181*, 1−17.
54. Mayoral, T., Medina, M., Sanz-Aparicio, J., Gomez-Moreno, C., and Hermoso, J. A. (2000) Structural basis of the catalytic role of Glu301 in Anabaena PCC 7119 ferredoxin-NADP(+) reductase revealed by x-ray crystallography, *Proteins: Struct., Funct., Genet., 38*, 60−69.
55. Massey, V. (1994) Activation of molecular-oxygen by flavins and flavoproteins, *J. Biol. Chem. 269*, 22459−22462.

BI061011T